

https://dspace.org/

The role of the particle size and distribution and its allied physical characteristics on the transportation of medium and dense phase slurries in South Africa

Verkerk, Cornelius Gerardus

2011-05-24
http://hdl.handle.net/10539/9901

Downloaded from a DSpace repository. https://dspace.org/

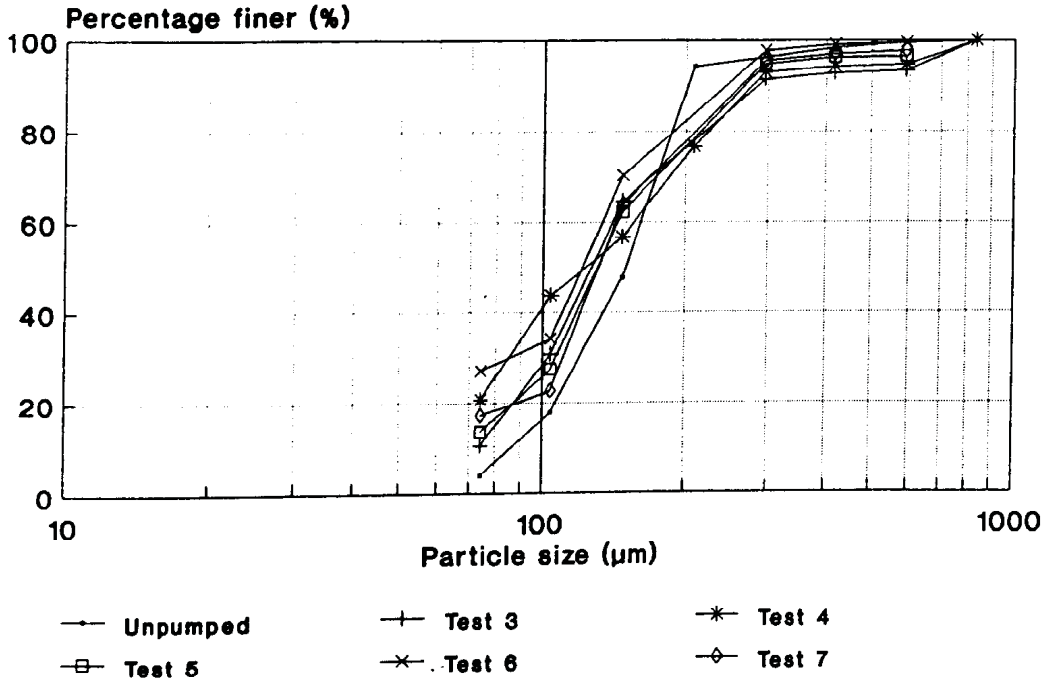


Figure 9.14 Size analysis of tails 16 samples

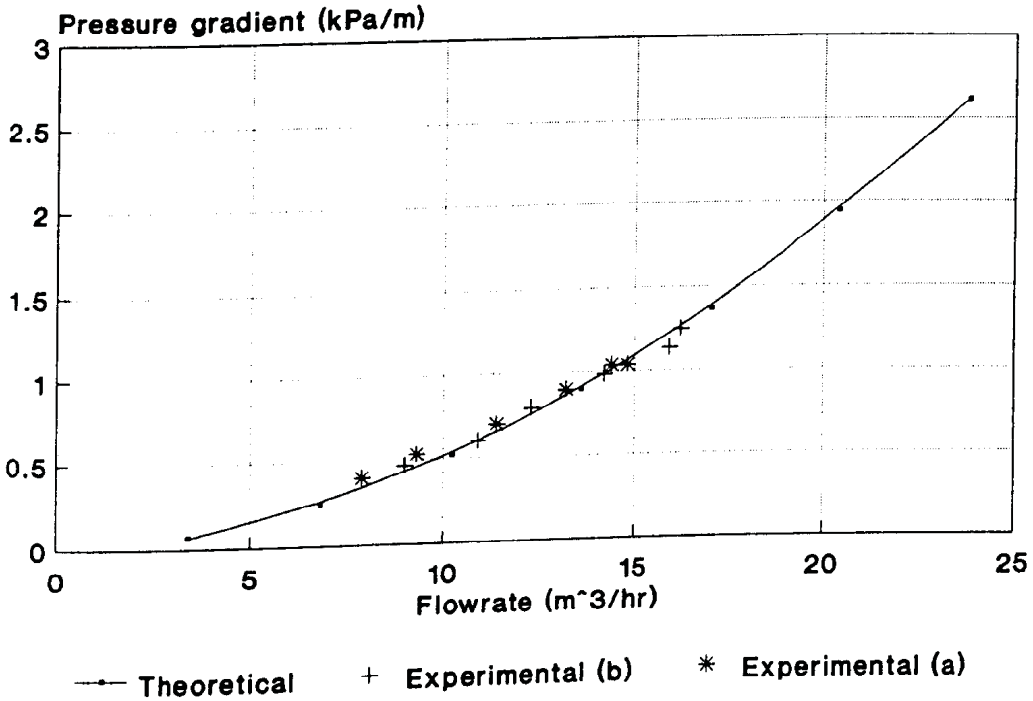


Figure 9.15 Clean water friction gradients for the 50 mm NB Schedule 80 pipeline

The friction gradients for the slurry tests (APPENDIX Z) are illustrated in Fig. 9.16 in terms of kPa/m and in terms of m_{sl}/100 m in Fig. 9.17.

The characteristic trend of increasing friction gradient with increasing slurry concentration and flowrate is again prevalent in Figs 9.16 and 9.17. It should be noted that the friction gradient in terms of m_{sl}/100 m is higher than the water friction gradient for all the slurries tested. A comparison of the size distribution of the tailings 16 product with tails products tested in Chapter 7 indicates that the tails 16 product is coarser than the tailings products tested in that chapter and coarser than the tails 14 product tested in Section 9.2. The tails 16 product is however finer than the tails 15 product.

A comparison of the friction gradient results obtained (Section 9.2, 9.3, 9.4) and the indication that Newtonian rheology would occur with this slurry, together with the resulting higher bed loads that could be expected, would indicate that higher friction gradients than the water gradients would be expected.

The movement of the various slurries tested through the 52 mm transparent viewing section was observed. The flow conditions observed are listed in the following Table (9.21).

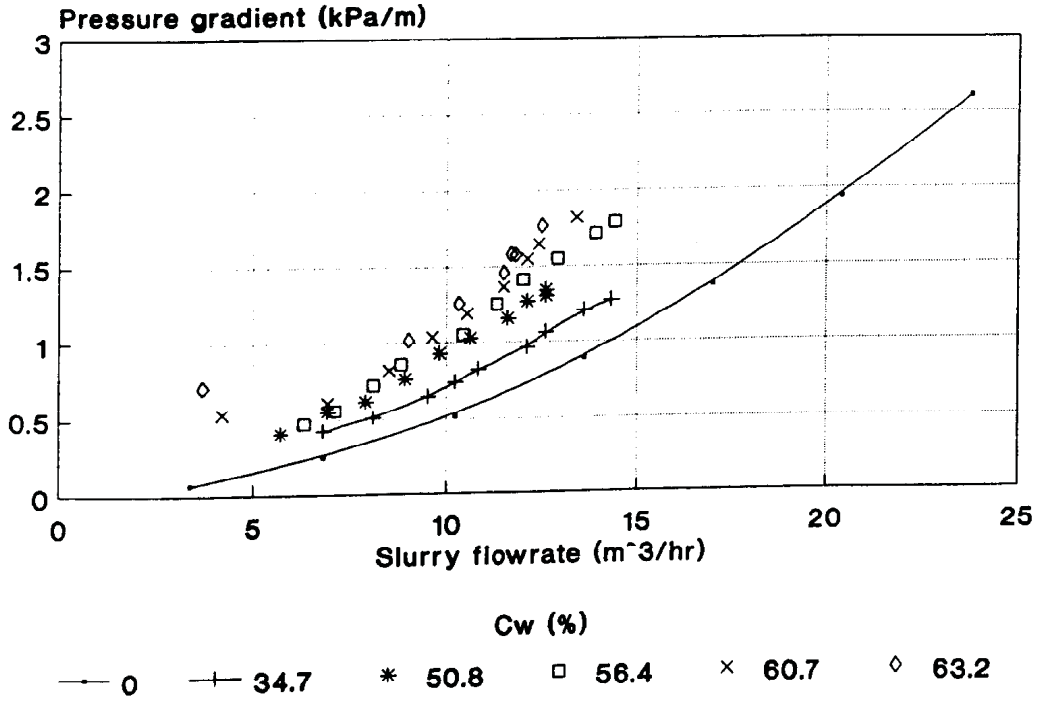


Figure 9.16 Slurry friction gradients (ID = 49mm)

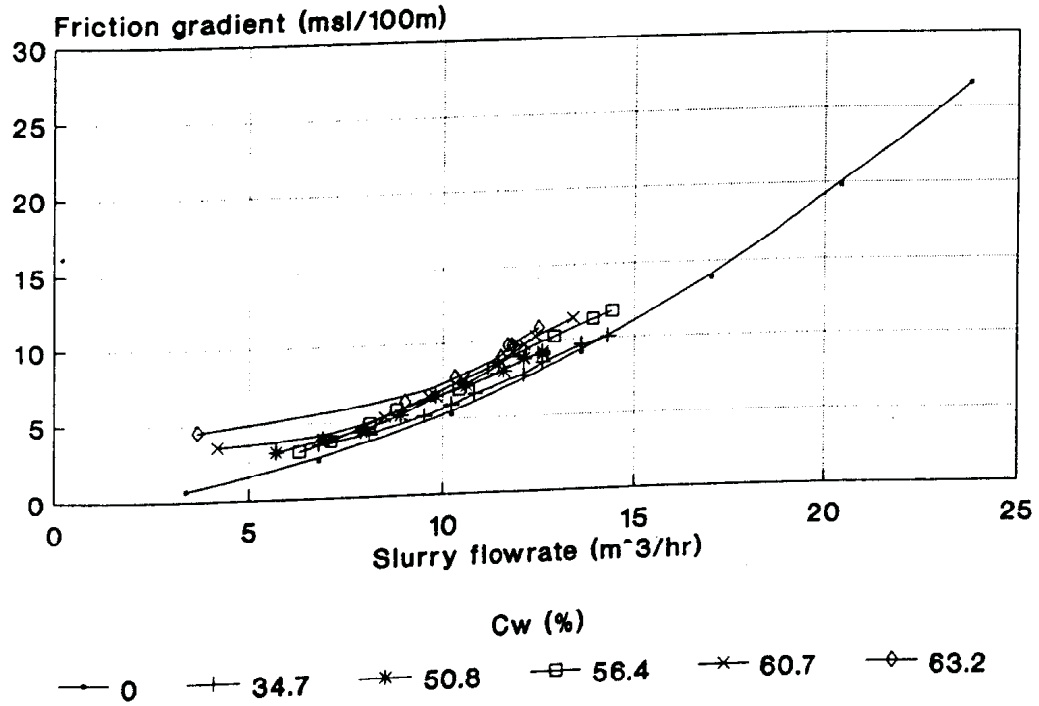


Figure 9.17 Slurry friction gradients (ID = 49 mm)

Table 9.21 Observed flowrates for various conditions in the pipeline

s.g	Flowrates (m^3/hr) (m/s)				
	Full flow	indication of saltation	saltation	moving bed	fixed bed
1,28	(1,34) 9,48		(1,14) 8,09		(0,97) 6,84
1,47	(1,38) 9,75	(1,26) 8,93	(1,11) 7,86		(0,81) 5,70
1,66	(1,76) 12,46	(1,67) 11,83	(1,46) 10,34	(1,27) 8,96	(0,52) 3,66
1,62	(1,48) 10,45	(1,36) 9,61	(1,20) 8,45	(0,97) 6,87	(0,59) 4,18
1,55	(1,25) 8,84	(1,14) 8,06		(1,00) 7,08	(0,88) 6,25

*( ) The values in brackets are the corresponding flow velocities.

From Table 9.21 above, the apparent trend is one of increasing velocity to maintain full flow conditions, with increasing concentration. This trend is consistent with other researchers work[126], where it has been shown that the velocity at the limit of the zone of a stationary bed is low for small solids concentrations, attains a maximum at an intermediate concentration and then decreases as the concentration becomes even larger.

Work by Wilson[126] indicates that for a sand slurry with a d_{50} = 180 μm the maximum deposit limit velocity is 1,25 m/s. If one considers the velocities shown in the last two columns of Table 1, then the value predicted by Wilson appears to indicate the maximum value of the deposit velocity in this test series.

One should however bear in mind that the condition of saltation in the pipeline is conducive to deposition in the pipeline and is influenced by other factors such as the inclination of the pipeline.

The suggested practice of adding 0,3 m/s to the deposition velocity to obtain the minimum transportation velocity would result in full flow conditions except for the slurry with a s.g = 1,66 where full flow occurs at a velocity in the region of 1,7 m/s.

The performance of the slurries, appears to require a prediction method which incorporates a Newtonian derived viscosity. Of the methods utilized in Section 9,2, the Lazarus method and the i_w x r.d method would appear to be unsuitable from the onset as the friction gradient curves (Fig. 9.17) do not asymptote to the clear water friction curves at high velocities. The Lazarus and Sive method (Section 5.53), Uhlmann (Section 5.51) Weber (Section 5.54) and Wasp method (Section 5.52) would all appear to be applicable for predicting the flow of the tails 16 product.

As no slip friction was measured it is not possible to apply the Lazarus and Sive method. The latter three methods are all based on similar concepts in that the flow is split into a carrier component and a heterogeneous carried component. As an illustrative exercise the Wasp method is compared to the experimental results in the following Tables (9.22 - 9.23). The modified Wasp method (Table 9.5) is not utilized as a comparison as rheological tests were found difficult to conduct due to the very small percentage of -74 µm material.

Table 9.22 Pressure gradient predictions for the tails 16 slurry flowing through a 49 mm pipeline

C_w (%) Velocity (m/s)	Pressure Gradient (kPa/m)					
	34,7		50,8		56,4	
	Experi-mental	Wasp	Experi-mental	Wasp	Experi-mental	Wasp
1,0	0,36	0,48	0,50	0,53	0,54	,55
1,5	0,72	0,74	0,94	0,90	1,02	,99
2,0	1,15	1,17	1,47	1,46	1,61	1,61
2,5		1,73		2,35		2,58

Table 9.23 Pressure Gradient predictions for the tails 16 slurry flowing through a 49 mm pipeline

C_w (%) Velocity (m/s)	Pressure Gradient (kPa/m)			
	60,8		63,5	
	Experimental	Wasp	Experimental	Wasp
1,0	0,64	0,54	0,81	0,58
1,5	1,09	1,11	1,21	1,22
2,0	1,82	1,87	1,97	2,00
2,5				
3,0				
3,5				
4,0				

The best approximation to the experimental values is obtained by varying the K value and the slurry viscosity used. The Durand K factor found to produce the best correlation of the data was 60.

The comparison of the viscosity data found to best fit the experimental data and the standard viscosity predictions is included in the following Table 9.24.

Table 9.24 Comparison of derived viscosity values for the tails 16 slurry

C_w (%)	Relative viscosity				
	Derived	Vand Roscoe Brinkman	Vand	Roscoe	Frankell Arcivos (ϕ_m:,66*)
34,7	1,9	1,6	1,6	1,9	1,9
50,8	3,9	2,3	2,3	3,2	3,4
56,4	5,2	2,7	2,8	4,3	4,2
60,8	6,5	3,1	3,3	5,5	5,2
63,2	8,0	3,5	3,6	6,5	6,0

*ϕ_m = ϕ_{max1}

The methods used above are listed in Table 5.1.

The Roscoe method best approaches the derived viscosity values but are still lower than the derived values. Use of a smaller ϕ_m with the Frankel & Arcivos method would give a better correlation. These results again indicate the influence of the particle shape, and size on the relative viscosity, and how a random selection of one of the above methods can lead to errors in predicting the friction gradient.

The prediction of the critical deposit velocities is based on the equations listed in Table 9.11. The resulting predictions are included in the following Table (9.25). The modified Durand and Wasp 1 predictions correlates the best with the experimental results.

Table 9.25 Predicted deposition velocities for an ID = 49 mm

C_w (%)	Deposition velocity (m/s)					
	Experimental deposit velocity	Durand	Modified Durand	Wasp 1	Wasp 2	Newitt
34,7	1,05	1,25	1,20	1,08	0,91	,85
50,8	,96	1,30	1,19	1,19	0,91	1,10
56,4	,91	1,30	1,17	1,17	0,91	1,19
60,8	,87	1,28	1,16	1,16	0,91	1,26
63,2	1,14	1,26	1,13	1,13	0,91	1,30

9.5 Tails 17

Pipeline tests were conducted with these quartz based tailings to establish the feasibility of transporting these slurries at relative densities up to 1,8. This slurry relative density is representative of a thick paste for full plant classified tailings. The tails 17 material has been cycloned to remove the fines to enhance the drainage characteristics of the slurry when used as a fill material.

The Malvern size distribution of the material is included in Table 9.26 and illustrated in Fig. 9.18.

Table 9.26 Tails 17 Size distribution analysis

Size (μm)	Cumulative percentage passing (%)
600	100
493	99,1
404	98,0
301	93,1
203	71,7
151	46,7
102	23,3
83,4	17,6
68,5	14,3
56,2	12,2
41,8	10,3
31,1	9,0
21,0	7,5
10,5	4,9
5,27	2,7
$\varnothing_{max\ 1}$ (%)	72,6
$\varnothing_{max\ 2}$ (%)	71,6

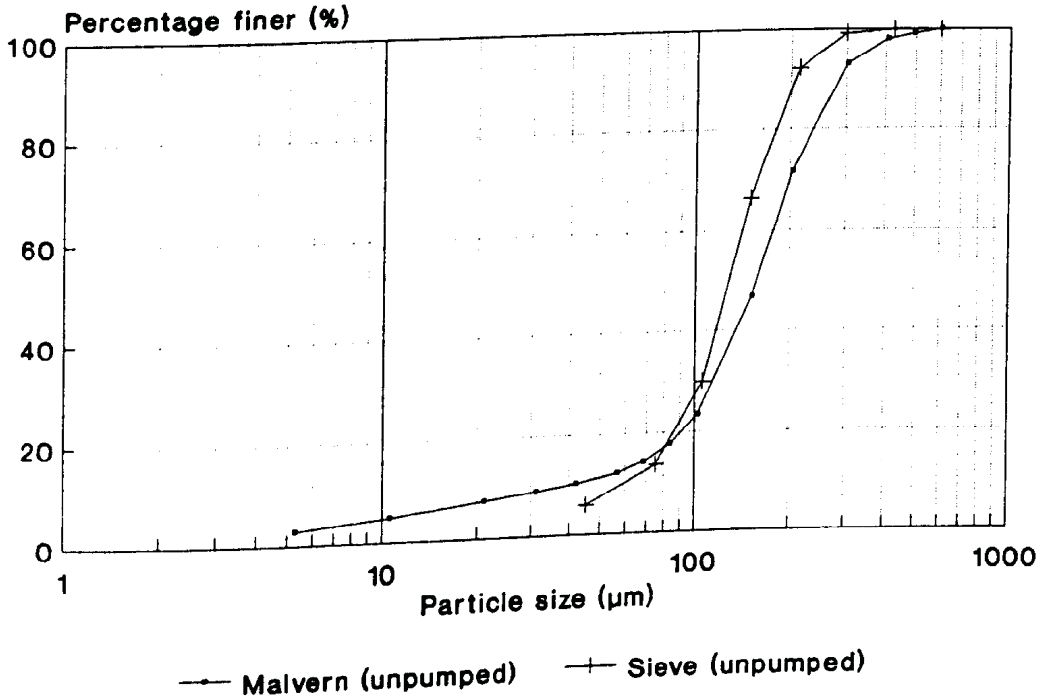


Figure 9.18 Size analysis of the tails 17 sample

Sieve analyses were also conducted on the tailings product, prior to being pumped and on samples taken during each pumping test.

The size analyses recorded are included in the following Table.

Table 9.27 Sieve size analysis of the tails 17 product

	Cumulative percentage passing %					
Text no	O	A	B	C	D	E
C_w (%)	O	59,2	62,1	66,3	60,0	67,7
Size (µm)						
600	99,9	100,0	99,9	99,9	100,0	100,0
425	99,8	99,8	99,7	99,8	99,9	99,8
300	99,2	99,2	99,2	99,1	99,3	99,1
212	92,3	92,3	92,2	92,2	92,7	92,2
150	66,4	66,1	66,0	64,6	66,0	64,2
106	29,7	28,6	29,0	27,3	27,9	26,9
75	13,6	11,7	12,5	11,2	11,4	11,2
45	5,9	4,2	5,0	4,0	4,2	3,9

The comparison between the sieve analysis and the Malvern analysis is illustrated in Fig. 9.18. This comparison serves to highlight that different size analysis techniques can result in different representative distributions.

The comparison between the size analysis conducted during the test program indicates little degradation (Fig. 9.19).

The average particle specific gravity was found to be 2,73. The experimental maximum loosely packed volume concentration was found to be 47,4% which is representa-

tive of a slurry density of 1,80.

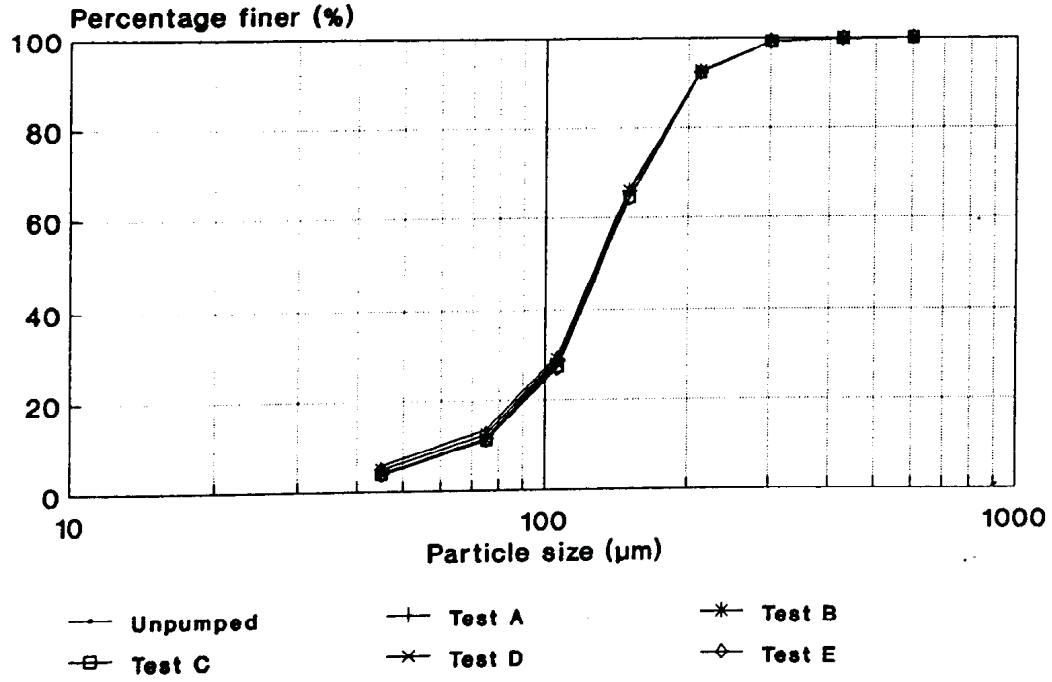


Figure 9.19 Size analysis of pumped tails 17 samples

The testwork was conducted directly after the tails 14 experiments so that the same pipe roughnesses as utilized in Section 9.2 were utilized in this section.

The 52 mm steel pipe friction gradient results (APPENDIX ZA) are illustrated in terms of kPa/m in Fig. 9.20 and in terms of m_{sl}/100 m in Fig. 9.21. The 158 mm test results are illustrated with the above mentioned vertical scales in Figs 9.22 and 9.23.

The kPa/m results for both pipelines illustrates the characteristic trend of increasing pressure gradient with an increase in velocity and solids concentration.

The test results in terms of m_{sl}/100 m indicate friction gradients that are higher than the friction gradients for clear water at all the flowrates and concentrations tested.

The mixed regime distribution of the tailings and the apparently low rheological characteristics resulted in critical deposit velocities being observed in the glass viewing sections in each pipeline. The velocity ranges representing the different flow conditions within the pipeline for the tests conducted are included in the following Table (9.28).

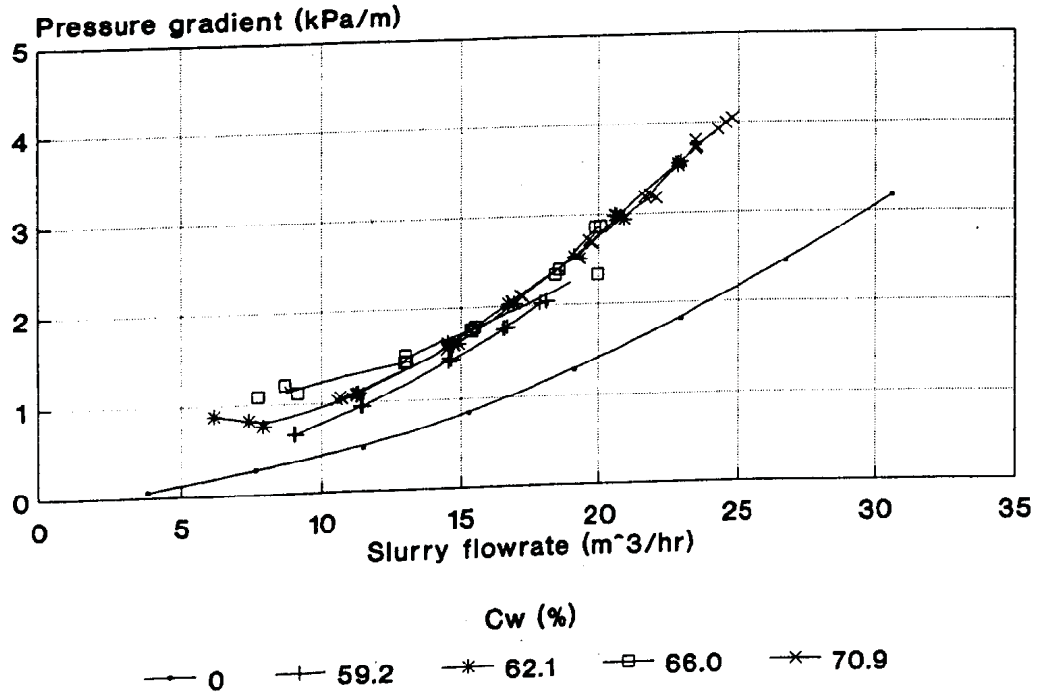


Figure 9.20 Tailings 17 friction gradients (ID = 52 mm)

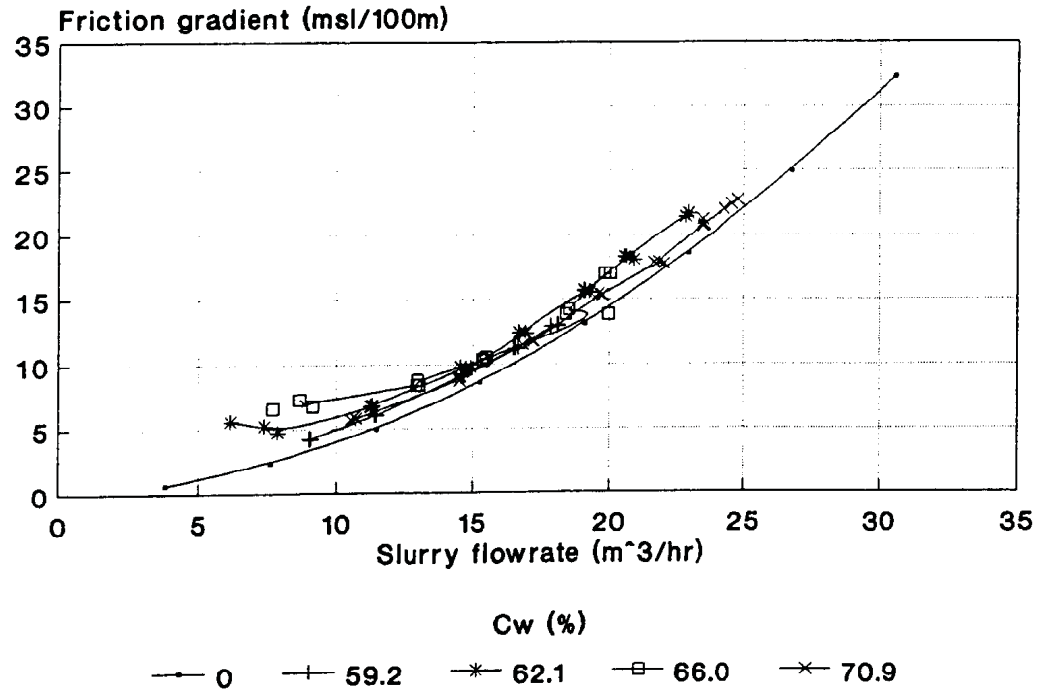


Figure 9.21 Tailings 17 friction gradients (ID = 52 mm)

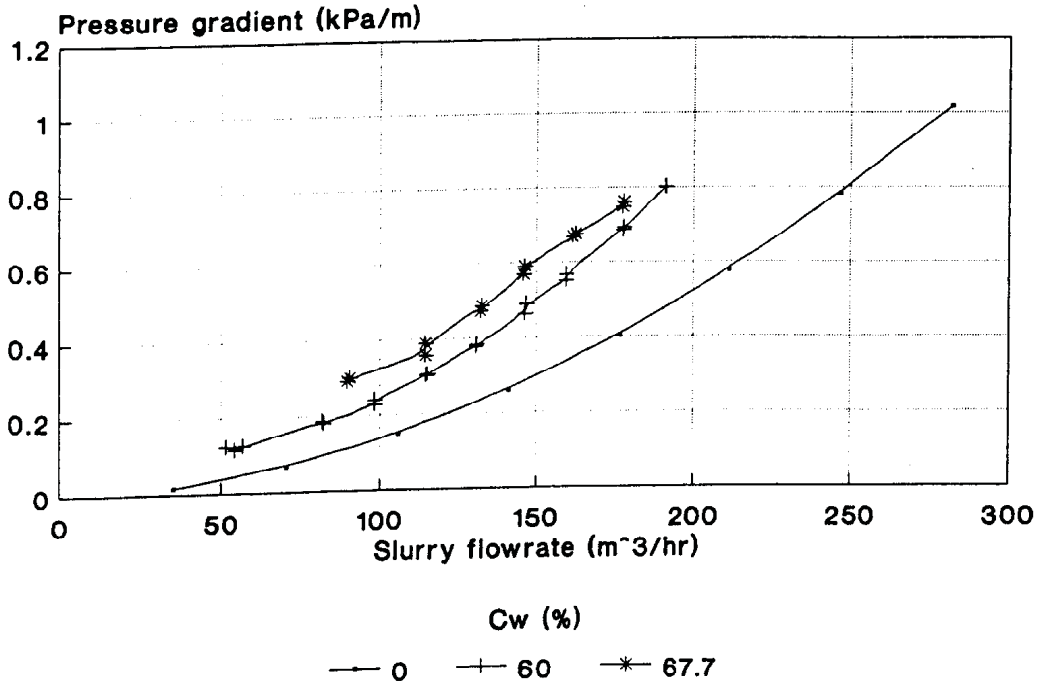


Figure 9.22 Tailings 17 friction gradients (ID = 158 mm)

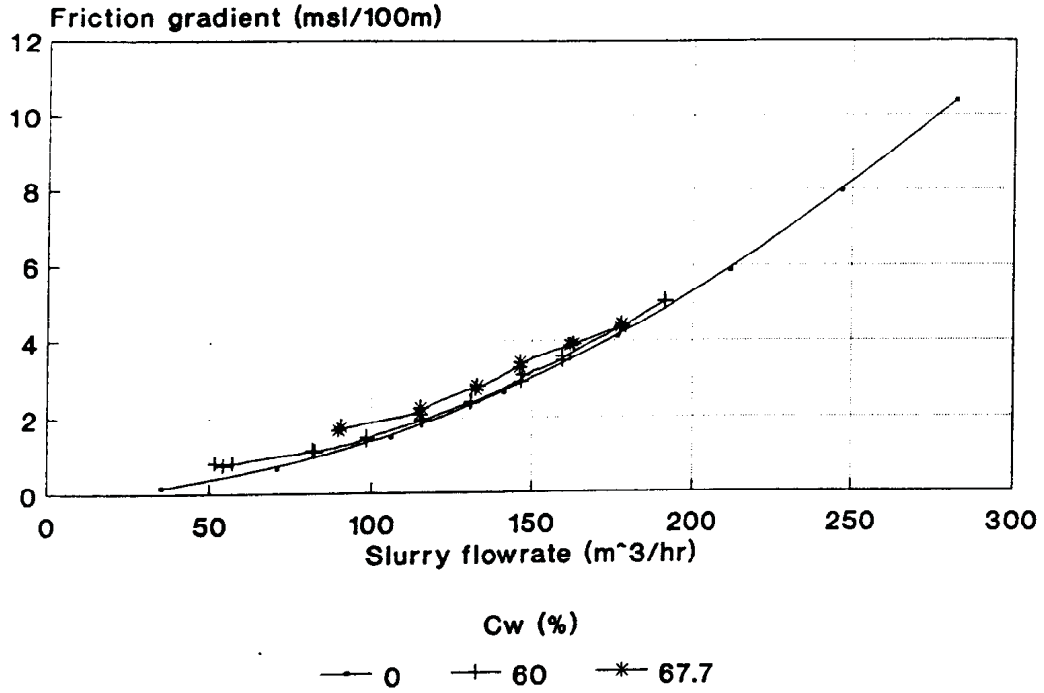


Figure 9.23 Tailings 17 friction gradients (ID = 158 mm)

Table 9.28 **Deposition and saltation flowrate characteristics**

Test C_w (%)	Pipe size (mm)	Flowrates (m^3/hr) (m/s)			
		Saltation		Deposition	
59,2	52	11,6	(1,52)	9,14	(1,20)
62,1	52	11,3	(1,47)	7,89	(1,03)
66,3	52	12,97	(1,70)	8,50	(1,11)
70,9	52	10,63	(1,39)		
60,7	158	99,66	(1,41)	88,26	(1,17)
67,7	158	110,09	(1,56)	88,40	(1,25)

* ( ) The values in brackets indicate the equivalent velocity for the full cross-sectional area of each pipe.

The deposition velocity occurs in a fairly consistent flow velocity band for the 52 mm and 158 mm pipelines. There is an increase in the expected deposition velocity with

an increase in pipe size.

As the friction gradient results indicated the relative importance of the rheology of the slurry, especially at the higher concentrations rheological tests were conducted on the samples taken for the size analysis comparison. The test rheograms and the derived stress-strain data are included in Appendix ZA.

The best models fitting the derived stress vs strain data best are included in the following Table. The composite comparative rheogram of the curves listed in Table 9.29 is illustrated in Fig. 9.24.

Table 9.29 Rheological models fitted

Test	C_w (%)	Model fitted (Pa)	Applicable strain rate range (1/s)
A	59,2	$\Gamma_w = ,03 + ,205\ S^{,750}$	35 < S < 286
B	62,3	$\Gamma_w = ,50 + ,186\ S^{,676}$	35 < S < 294
C	66,3	$\Gamma_w = ,35 + ,550\ S^{,6078}$	45 < S < 375
D	60,0	$\Gamma_w = ,2994 + ,5343\ S^{,556}$	18 < S < 153
E	67,7	$\Gamma_w = ,374 + 1,022\ S^{,5022}$	41 < S < 393

A plot of the constant shear rate curves for increasing concentration is illustrated in Fig. 9.25. The curves again illustrate the asymptotic tendency of the trends established in Section 7.

As the slurry indicated settling tendencies during the test program, the same basic prediction formuli utilized in Section 9,2 are utilized in this section to compare predicted friction gradients with the experimental results. The predictions based on the Wasp, Modified Wasp,

i_w x r.d and Lazarus are included in the following Tables (9.30 - 9.34).

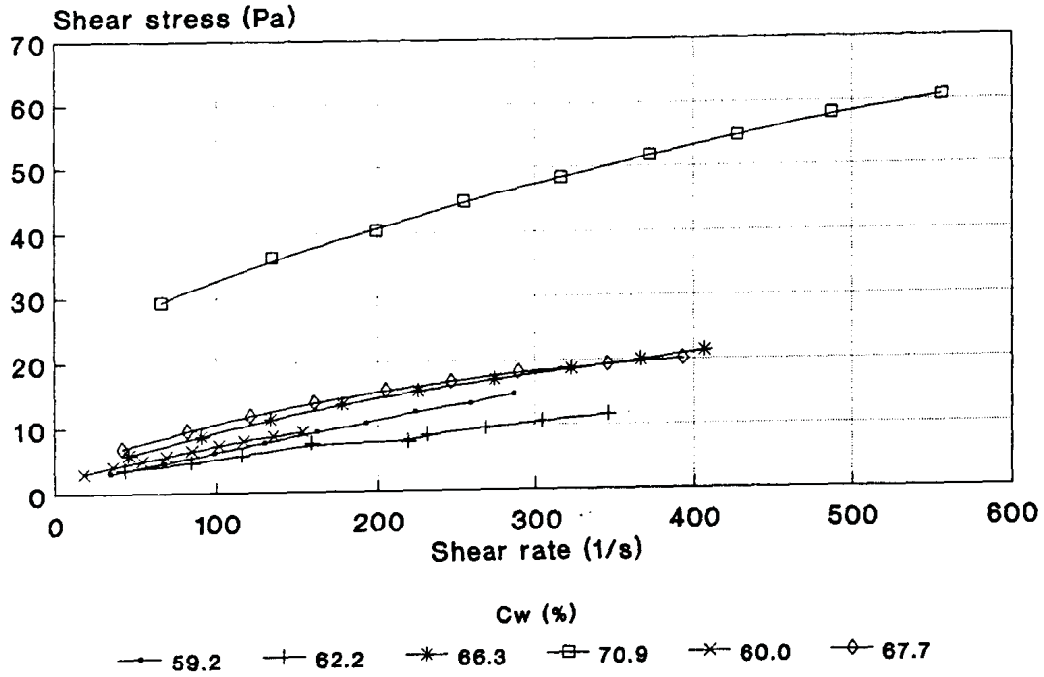


Figure 9.24 Comparative pumped tails 17 rheogram

Table 9.30 Pressure Gradient Predictions for a C_w = 59,2% slurry flowing in a 52 mm pipeline

Velocity (m/s)	Pressure Gradient (kPa/m)			
	Average Experi-mental	Wasp	i_w x r.d	Lazarus
1,0	,50	,490	,363	,476
1,5	,95	,897	,776	,800
2,0	1,51	1,633	1,338	1,338
2,5	2,22	2,434	2,049	2,049
3,0		3,388	2,909	2,909
3,5		4,495	3,916	3,916

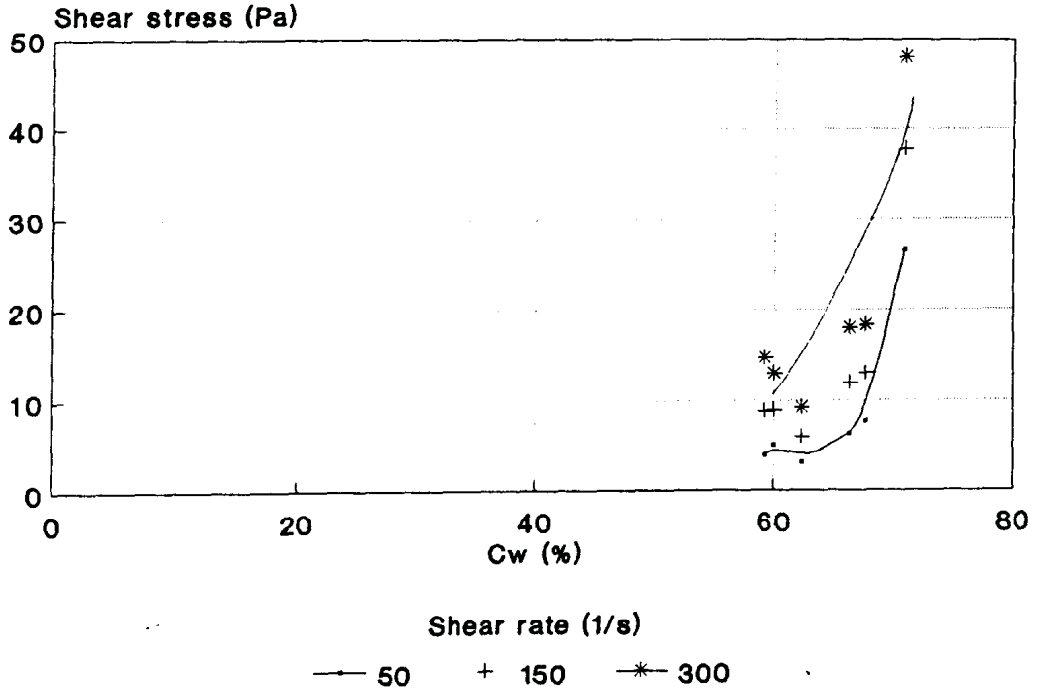


Figure 9.25 Constant shear rate curves for the pumped tails 17 slurries

Table 9.31 Pressure Gradient Predictions for a C_w = 62,3% slurry flowing in a 52 mm pipeline

Velocity (m/s)	Pressure Gradient (kPa/m)				
	Average Experimental	Wasp	Modified Wasp	i_w x r.d	Lazarus
1,0	,82	,509		,375	,482
1,5	1,12	,959	1,213	,802	,806
2,0	1,72	1,732	1,86	1,382	1,379
2,5	2,52	2,578	2,62	2,116	2,111
3,0	3,56	3,583	3,49	3,004	2,997
3,5		4,746	4,46	4,043	4,035

Table 9.32 Pressure Gradient Predictions for a C_w = 66,3% slurry flowing in a 52 mm pipeline

Velocity (m/s)	Pressure Gradient (kPa/m)				
	Average Experimental	Wasp	Modified Wasp	i_w x r.d	Lazarus
1,0	1,10	,548		,392	,489
1,5	1,29	1,162		,837	,837
2,0	1,85	1,918	2,292	1,442	1,443
2,5	2,67	2,847	3,146	2,208	2,209
3,0		3,945	4,113	3,135	3,135
3,5		5,209	5,166	4,220	4,221

Table 9.33 Pressure Gradient Predictions for a C_w = 60,0% slurry flowing in a 158 mm pipeline

Velocity (m/s)	Pressure Gradient (kPa/m)				
	Average Experimental	Wasp	Modified Wasp	i_w x r.d	Lazarus
1,0	0,16	,219	,177	,108	,171
1,5	0,27	,289	,311	,239	,291
2,0	0,44	,443	,472	,420	,430
2,5	0,69	,658	,660	,650	,650
3,0	1,00	,928	,870	,930	,931
3,5					

Table 9.34 Pressure Gradient Predictions for a C_w = 67,7% slurry flowing in a 158 mm pipeline

Velocity (m/s)	Pressure Gradient (kPa/m)				
	Average Experimental	Wasp	Modified Wasp	i_w x r.d	Lazarus
1,0				,117	,175
1,5	,35	,304	,360	,259	,298
2,0	,53	,506	,535	,456	,456
2,5	,78	,812	,732	,706	,706
3,0	1,10	1,140	,960	1,009	1,011
3,5				1,368	1,370

The friction gradients plotted in terms of m_{sl}/100m indicate that the water based prediction formuli would be applicable to these results, as all the friction gradients recorded had higher gradients, than the water curve.

The i_w x r.d prediction formuli therefore would be expected to under predict the friction gradients. Tables 9.30 - 9.34 show that this is the case.

The predicted values using the Wasp method and the modified Wasp method would appear to offer the best methods for determining the expected friction gradients. Both methods make use of rheologically based 'carrier' medium and as shown by the test results the friction gradients (Fig. 9.21) do not asymptote to the clean water curve.

A comparison of the size distribution of the tailings 17 product with the quartz based tailings products (Chapter 7) indicates from a global point of view that, Newtonian type rheology can be expected for the medium range of concentrations, C_v = 20 - 35% and non-Newtonian rheology

for the higher concentrations. The tailings 17 product has a higher d_{50} than the tailings tested in Section 7 so that the curves for the equivalent C_v could be expected to lie below the rheogram of the different tailings plotted in Figs 7.38 - 7.43. A comparison of the tailings 17 results indicates that this is the case. The Newtonian based predictions, provided the correct viscosity prediction method is utilized, can therefore be expected to result in a reasonable prediction.

The low rheological characteristics and the relative coarseness of the slurry can also be expected to result in a slurry characterised by a critical deposit velocity. This characteristic is evident from the critical velocities recorded in Table 9.28.

The estimation of the critical velocity is based on the methods listed in Table 9.11.

The predicted values are included in the following Table (9.35).

Table 9.35 Predicted deposition velocities

C_w (%)	I.D (mm)	Deposition velocity (m/s)						
		Experimental deposit velocity	Durand	Modified Durand	Wasp 1	Wasp 2	Thomas	Newitt
59,2	52	1,41	1,36	1,29	1,29	,95	,90	1,32
62,1	52	1,32	1,36	1,28	1,31	,95	,93	1,38
66,3	52	1,00	1,34	1,28	1,34	,95	1,00	1,45
60,7	158		2,36	2,14	1,89	1,37	1,04	2,35
67,7	158	1,50	2,34	2,14	1,95	1,37	1,17	2,58

The Durand and Newitt equations correspond closely to the 52 mm pipeloop, experimental test results. These however overpredict the critical deposit velocity by the order of 56% for the 158 mm pipeline. The closest predicted results for the 158 mm pipeline are based on the Wasp 2 prediction method.

The tailings 17 product slurries can be characterised as a mixed regime settling slurry and by Newtonian fluid based prediction formuli.

9.6 PFA2 and BBA slurries

Pipeline tests were conducted on the coarse BBA sample at concentrations up to 35% and mixtures of BBA and PFA up to C_w = 50% and the PFA only up to C_w = 55% in a 200 mm nominal bore pipeline. Two types of pipe surfaces were utilized. The steel pipe had an internal diameter of 206 mm while the rubberlined pipe had an ID = 192 mm.

The tests conducted represent the planned operating conditions of the ash disposal system at Matla power station. The rheological analysis of the PFA slurries corresponding to these pipeline tests are included in Section 7.42 and 7.43.

The PFA and BBA slurries were previously transported at concentrations of 20 and 5 - 10% respectively. The location of the mine under the existing ash dam has necessitated the move of the ash dam to a depression approximately 5 km from the power station.

The natural production of the two ash products is in a ratio of 8:2 PFA to BBA. To optimize the disposal system

it has been proposed to transport the two products as a single slurry at concentrations of the order of 50 - 55%, bearing in mind that the range of operating conditions at the powerstation was such that the slurry could vary from a pure PFA slurry to a pure BBA slurry.

The rheological analysis of the PFA (Sections 7.42 and 7.43) indicated that a steep rise in the rheological characteristics could be expected above concentrations of 50%. This value was thus used as a basis for the testwork conducted.

The size distributions of the unpumped PFA and BBA used in the pipeline tests is included in the following Tables (9.36 - 9.37) and illustrated in Fig. 9.26.

Table 9.36 PFA 2 Size distribution

Size (μm)	Cumulative percentage passing (%)
564	100
262	99,4
160	94,6
113	88,0
84	79,6
50	63,1
30	48,5
18	34,0
11	23,1
9,1	19,1
5,8	12,2
$\phi_{max\ exp}$ (%)	46,1
$\phi_{max\ 1}$ (%)	98,9
$\phi_{max\ 2}$ (%)	80,9

Table 9.37 BBA Size distribution

Size (μm)	Cumulative percentage passing (%)
6300	94,1
4750	91,7
2360	83,0
1180	69,7
600	56,4
212	30,6
106	10,5
$\varnothing_{max\ exp}$ (%)	38,9
$\varnothing_{max\ 1}$ (%)	78,0
$\varnothing_{max\ 2}$ (%)	86,5

The pipeline tests were conducted on a range of concentrations ranging from 43 to 56%. The PFA:BBA ratio's included in the study were 1:1, 2:1 and 4:1.

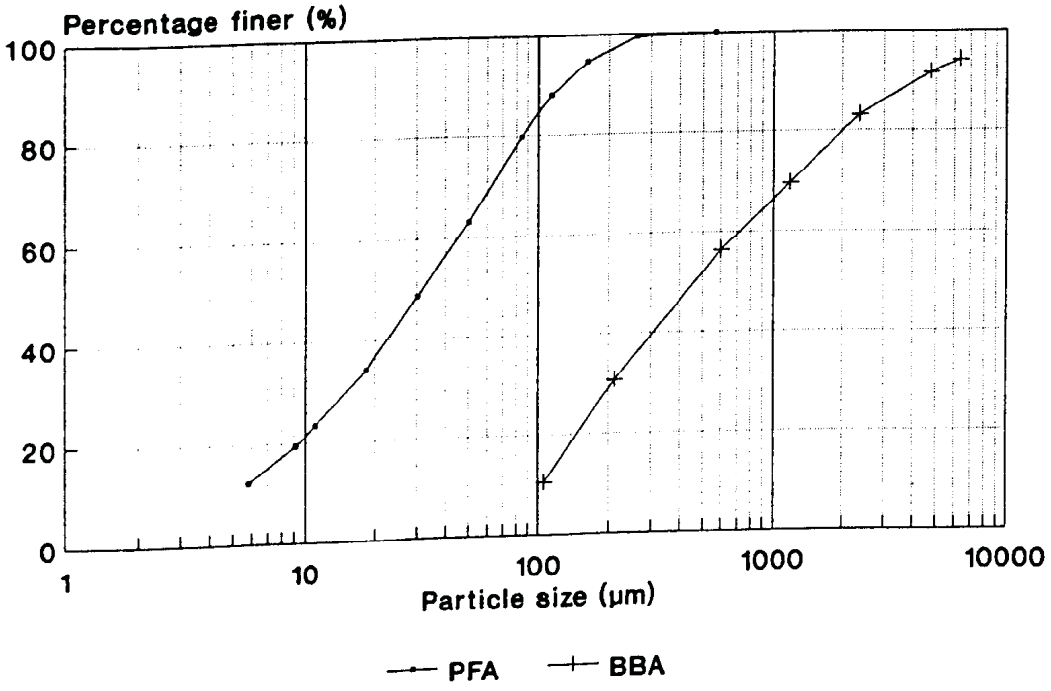


Figure 9.26 PFA and BBA Size distributions

Prior to and after the slurry tests, tests were conducted with water to establish the average roughness ratio's of the two pipe surfaces utilized in this test series.

The experimental results of these tests are illustrated in Fig. 9.27. Successive iterations of the Colebrook-White equation[1] resulted in k/d values of 0,0001 and 0,00045 for the rubberlined and steel pipe respectively. The roughness ratio's were determined over a 45 m length of piping which included 6 joints for both the rubberlined pipe and the steel pipe. The roughness ratio for the steel pipe is higher than could be expected for a clean steel pipe. The corroded condition of the steel pipe prior to these tests is illustrated in Fig. 9.28.

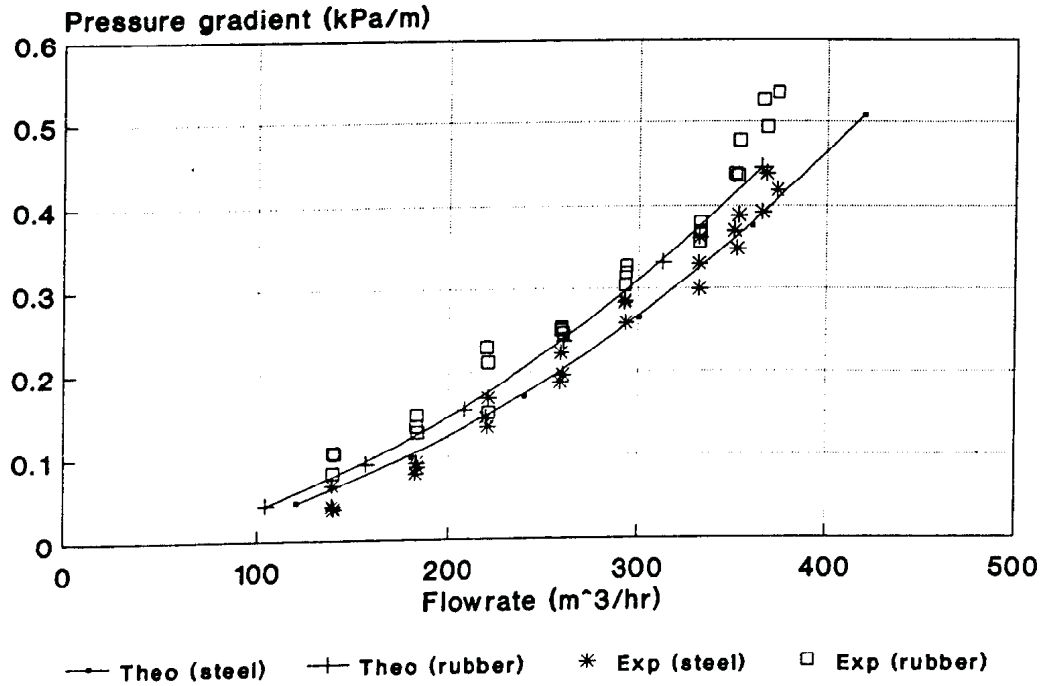


Figure 9.27 Predicted and experimental water pressure gradients

Tests prior to and after the slurry tests revealed no change in the derived roughness ratio's.

The pressure gradients for the PFA slurries (APPENDIX ZB) tested are illustrated in Figs. 9.29 - 9.32 in terms of kPa/m and m_{sl}/100 m for the rubberlined and steel pipes respectively.



Figure 9.28 Internal surface of the steel pipe

The characteristic trend revealed by the kPa/m curves is one of an increasing pressure gradient with an increase in concentration and slurry flowrate. The curve for a C_w = 56% slurry (Fig. 9.21) tends to confirm the increasing rheological trends indicated from the rheological analysis.

The diverging nature of the curves illustrated in Figs. 9.30 & 9.32 would also tend to corroborate the yield pseudoplastic characteristics obtained from the rheological tests.

The pressure gradients for slurry concentrations in the region of 50% for the mixture slurries are illustrated in Figs. 9.33 & 9.34. A feature of these curves is the flattening out of the curves near the deposition velocity of each slurry and the increase in the pressure gradient at the higher flowrates as the percentage of PFA is increased.

The results are also characterised by an increase in the deposition velocity as the percentage of BBA is increased in the mixture. Two tests on the 1:1 ratio of PFA to BBA at C_w = 50% and 40% revealed a higher deposition velocity for the lower concentration slurry. It would appear that the concentration is important at this mixture ratio as the limit of the enhanced carrying capacity of the PFA based carrier and the turbulence required to support the coarser BBA particles occurs in the concentration range of 40% - 50%.

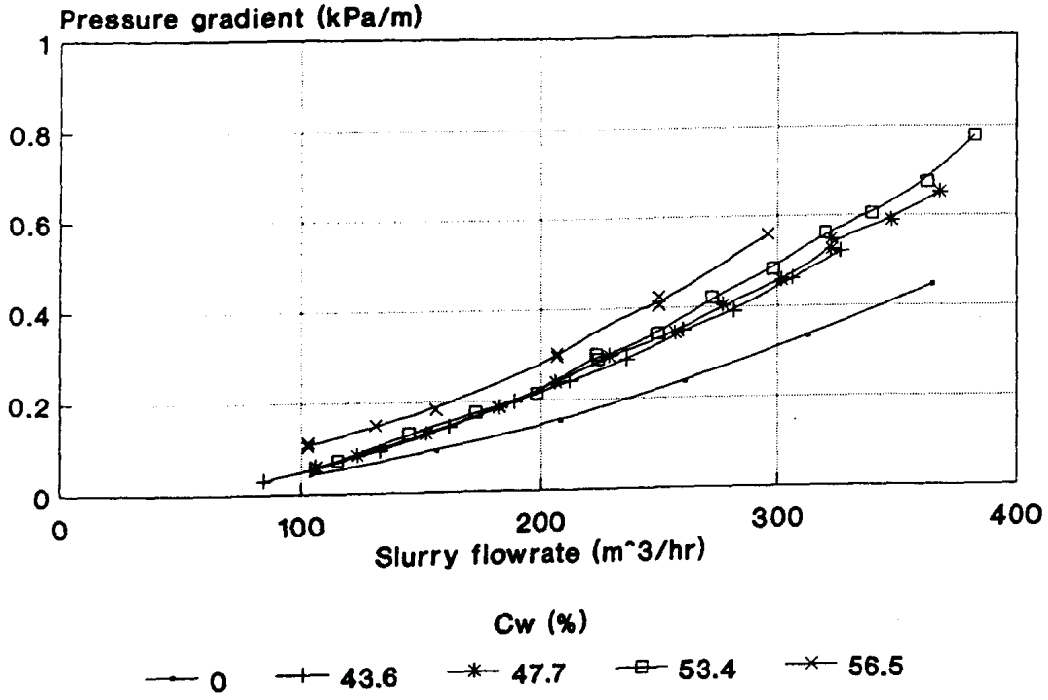


Figure 9.29 PFA 2 Friction gradients (rubber)

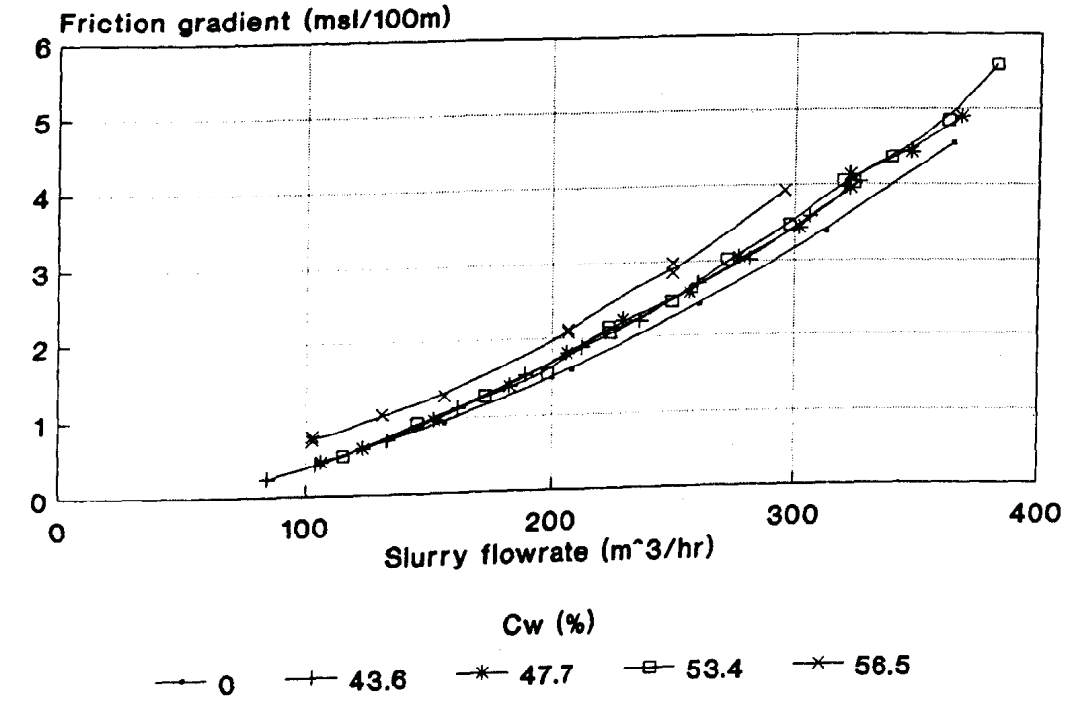


Figure 9.30 PFA 2 Friction gradients (rubber)

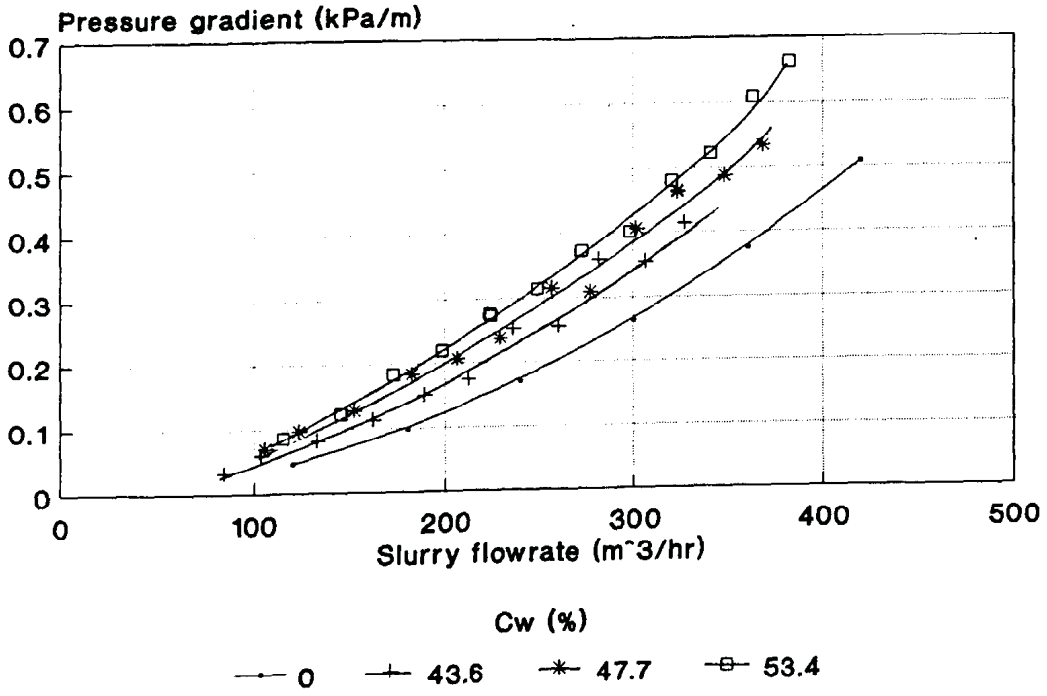


Figure 9.31 PFA 2 Friction gradients (steel)

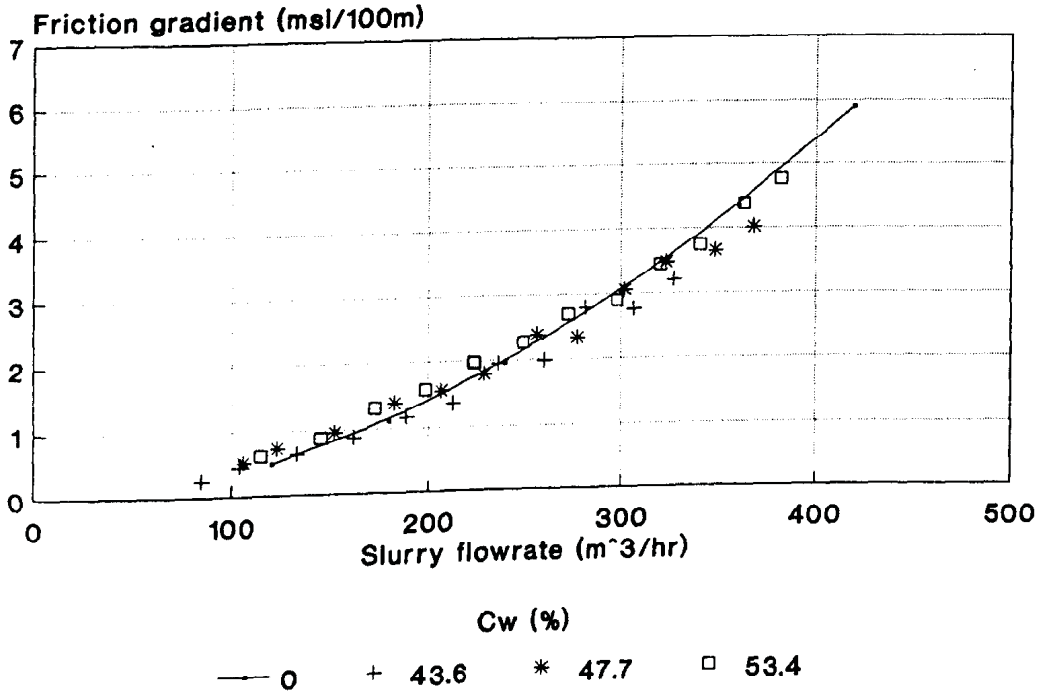


Figure 9.32 PFA 2 friction gradients (steel)

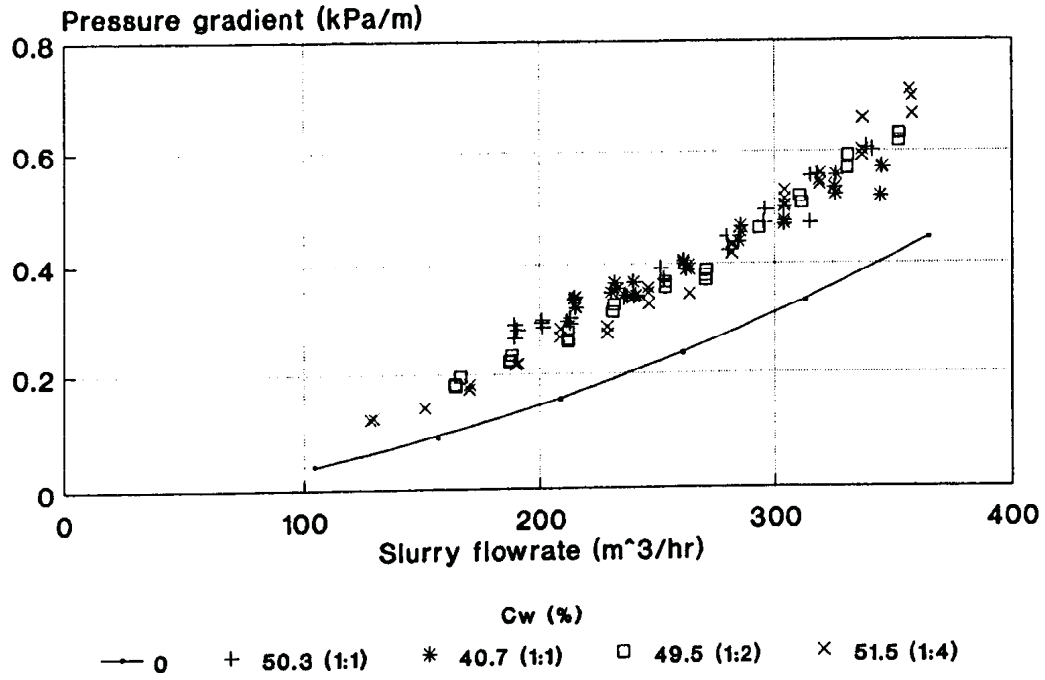


Figure 9.33 Mixture pressure gradients (rubber)

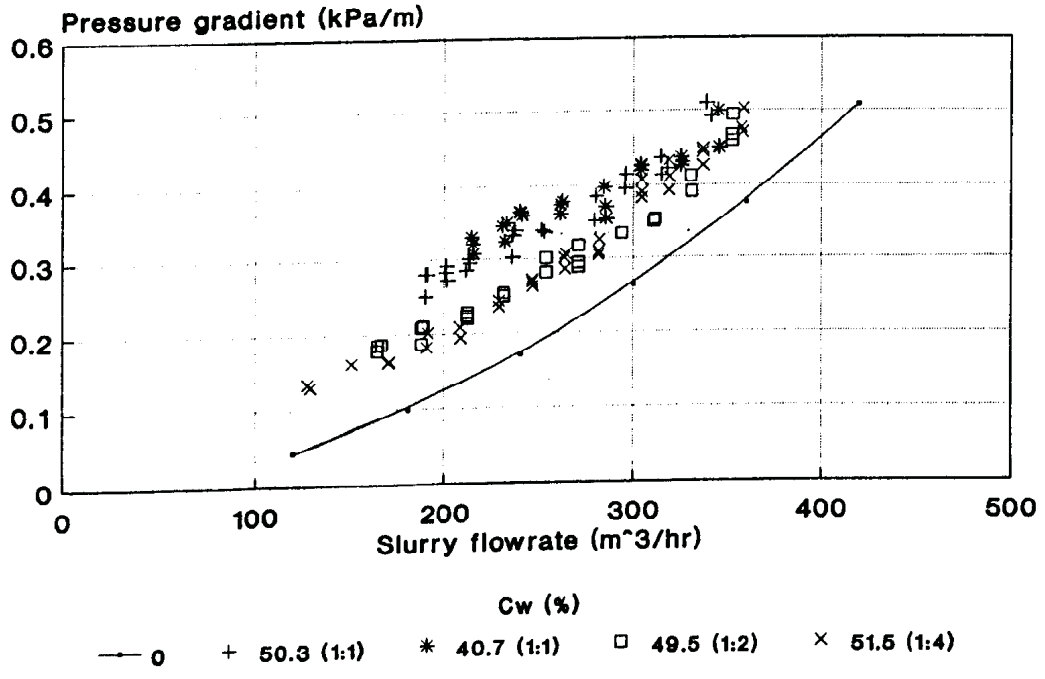


Figure 9.34 Mixture pressure gradients (steel)

The degradation occurring during the mixture tests appears to be less than that apparent from the BBA tests. Size analysis and the friction analysis of two tests of the 1:1 ratio revealed similar results.

The size distributions of the PFA:BBA mixtures are included in the following Tables. The PFA distribution is given in Table 9.36.

Table 9.38 Size analysis of the PFA:BBA mixtures transported

Sieve size (μm)	Cumulative percentage passing (%)					
	BBA : PFA 1 : 1		BBA : PFA 1 : 2		BBA : PFA 1 : 4	
	Estimated distribution	Actual distribution	Estimated distribution	Actual distribution	Estimated distribution	Actual distribution
6300	98,5	98,0	98,0	99,8	98,8	99,9
4750	97,7	97,1	97,2	99,7	98,3	99,7
2360	94,0	92,4	94,3	97,9	96,6	98,5
1180	87,4	84,1	89,9	93,5	94,0	95,9
600	80,1	75,5	85,5	87,7	91,4	92,5
212	67,1	59,8	75,1	73,9	84,0	81,2

The estimated distributions for the 1:1 tests are calculated from the BBA distribution of the BBA remaining in the pumping circuit after the last BBA test (Table 9.39). The remaining estimations are based on the original material distributions as fresh material was used for the 1:2 and 1:4 tests. The distributions are illustrated in Fig. 9.35.